Vortex fluidic mediated synthesis of TiO2 nanoparticle/MXene composites

Journal Item

CHEMNANOMAT

CHEMISTRY OF NANOMATERIALS FOR ENERGY, BIOLOGY AND MORE

www.chemnanomat.org

Accepted Article

Title: Vortex fluidic mediated synthesis of TiO2 nanoparticle/MXene composites

Authors: Ahmed Hussein Mohammed Al-Antaki, Thaar M. D. Alharbi, Suela Kellici, Nicholas P. Power, Warren D. Lawrance, and Colin L. Raston

To be cited as: *ChemNanoMat* 10.1002/cnma.201900779

Link to VoR: http://dx.doi.org/10.1002/cnma.201900779

A Journal of

ACES Asian Chemical Editorial Society

A sister journal of **Chemistry – An Asian Journal** and **Asian Journal of Organic Chemistry**

WILEY-VCH

10.1002/cnma.201900779

WILEY-VCH

FULL PAPER

Vortex fluidic mediated synthesis of TiO_2 nanoparticle/MXene composites

Ahmed Hussein Mohammed Al-antaki[a,b], Thaar M. D. Alharbi[a], Suela Kellici[c] , Nicholas P. Power[d], Warren D. Lawrance[e], Colin L. Raston*[a]

[a] Ahmed Hussein Mohammed Al-antaki, Thaar M. D. Alharbi, Prof. Colin L. Raston, Flinders Institute for Nanoscale Science and Technology, College of Science and Engineering, Flinders University, Adelaide, SA 5042, Australia, alan0192@flinders.edu.au, alha0190@flinders.edu.au , Colin.raston@flinders.edu.au .

[b] Ahmed Hussein Mohammed Al-antaki, Department of Chemistry, Faculty of Sciences, University of Kufa, Kufa, Najaf, Iraq. Ahmed.alantaki@uokufa.edu.iq .

[c] A/Prof. Suela Kellici, School of Engineering London South Bank University, 103 Borough Road London, SE1 0AA (UK), kellicis@lsbu.ac.uk .

[d] Dr. Nicholas P. Power, School of Life, Health & Chemical Sciences, The Open University, Walton Hall, Milton Keynes, MK7 6AA (UK), nicholas.power@open.ac.uk .

[e] Prof. Warren D. Lawrance, College of Science and Engineering, Flinders University, Adelaide, SA 5042, warren.lawrance@flinders.edu.au .

Abstract: Oxidation of MXene in a vortex fluidic device (VFD) operating under continuous flow results in exfoliation and fragmentation into nanoparticles of surface oxidised 2D material with further oxidation of the nanoparticles into anatase (TiO_2). These MXene and anatase nanoparticles co-assemble into stable micron sized spheres which are topologically smooth, decorating the surface of exfoliated MXene. The formation of this composite material in the dynamic thin film in the VFD was optimised by systematically exploring the operating parameters of the microfluidic platform, determined at 45° tilt angle for the 20 mm diamater glass tube spinning at 5k rpm, with a flow rate of a colloidal dispersion of MXene in aqueous H_2O_2 (30%) at 0.75 mL/min, concentration of MXene 0.5 mg/mL.

Introduction

The first report describing the new and unique class of 2D MXene materials was in 2011.[1] They are based on transition metal carbides, carbonitrides and nitrides, and have potential in a number of applications, including in biological,[2-5] batteries,[6-8] electronic devices [9-10] and supercapacitors.[10-11] The unit formula of these materials is $M_{n+1}X_nT_x$ in which M is an early transition metal, including Sc, Ti, Cr, Zr, Nb, Mn, Mo, Hf, V, Ta, or W, X represents either carbon and/or nitrogen, and n is 1, 2, or 3 in defining the number of M layers. T_x represents surface functional groups −O, −OH, −F bound to the transition metals.[12-13] More than twenty types of MXenes have been developed, including Ti_2CT_x, $Ti_3C_2T_x$, V_2CT_x, Nb_2CT_x, Mo_2CT_x and Ti_3CNT_x.[14] Some of them contain two different transition metals, for example in $Mo_2TiC_2T_x$.[15-16] There is growing interest in nanocomposite materials involving MXenes, for example MXene ($Ti_3C_2T_x$)/α-Fe_2O_3 for use as a negative electrode material for supercapacitors,[17] MXene ($Ti_3C_2T_x$)/MnO_2 for high performance electrode materials for flexible supercapacitors,[18] and Ti_3C_2-MnO_2 for enhancing interfacial electronic coupling.[19] In addition, MXenes decorated with TiO_2 quantum dots (QDs) feature in Li-S batteries,[20] MXene-Cu_2O catalyses the thermal decomposition of ammonium perchlorate,[21] MXene-enzyme feature in electrochemical biosensors,[22] MXenes-CNTs improve electrochemical performance,[8] and MXene-Pt nanoparticles have sensing application[23] with others for determining ion exchange capacity.[24] More specifically, TiO_2 nanoparticle (NP)/MXene composites feature in rendering MXene biocompatible for enzyme attachment,[22] enhancing the efficiency of MXene modified glassy carbon electrodes for H_2O_2 reduction,[25] nitrite detection,[26] low detection limits of glucose[27] and sodium alanate,[28] Li-ion battery anodes[29] and photocatalysis.[30] Thermal methods have been used to oxidize MXene to TiO_2 or TiO_2NPs/MXene.[28, 30-31] with H_2O_2 also effective in preparing the same material.[29] Herein we report the oxidation of MXene (Ti_2C) in 30% H_2O_2 in gaining access to TiO_2 NPs/MXene composite materials, which encompasses exfoliation with surface oxidation, fragmentation of the 2D material, and oxidation of the fragmented material, using a vortex fluidic device (VFD). The VFD is a thin film microfluidic platform which has two types of processing, the confined mode where a glass tube, usually inclined at 45° relative to the horizontal position, is spun at high speed.[32] This is a proven approach for then translating any reaction into a continuous flow process, which is the other mode of operation of the VFD, Fig. 1.[33] The VFD is a versatile thin film device effective for a growing number of applications,

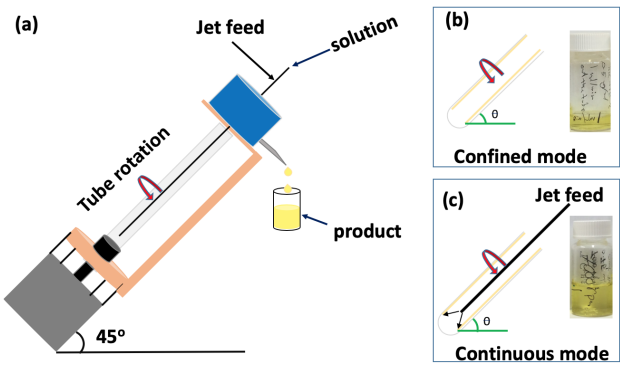

Fig. 1. (a) Diagrammatic representation of the VFD, for which the optimal processing in a 20 mm O.D. (17.5 mm I.D.) borosilicate glass tube is 5k rpm with a jet feed delivering a solution of MXene in aqueous H_2O_2 (30%), 0.5 mg/mL, flow rate 0.75 mL/min. Also shown are photographs of solutions produced using (b) the confined mode of operation of the VFD, and (c) continuous flow.

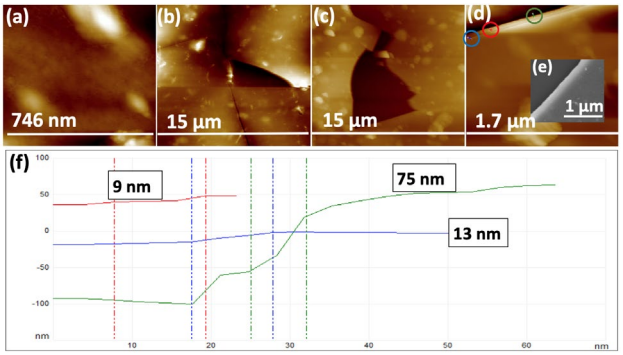

Fig. 2. AFM images for TiO_2 NPs/MXene composite drop cast onto silicon wafers and then oven dried at 60ºC, prepared from MXene dispersed in 30% H_2O_2 (0.5 mg/mL) with the optimal VFD of processing parameters as rotational speed 5k rpm, tilt angle 45º, flow rate 0.75 mL/min. (a-d) AFM images for TiO_2 NPs/MXene sheets. (e) SEM image for TiO_2 NPs/MXene sheets. (f) AFM height profile for TiO_2 NPs/MXene sheets.

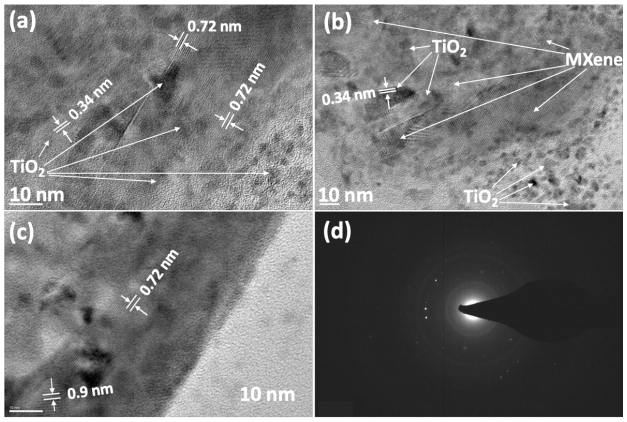

Fig. 4. HRTEM images for TiO_2 NPs/MXene drop cast on a grid, MXene in H_2O_2 (0.5 mg/mL) optimal of VFD processing at 5k rpm rotational speed, tilt angle 45º and flow rate 0.75 mL/min. (a-c) HRTEM. (d) SAED for TiO_2 NPs/MXene composite.

including *in situ* decorating *h*-BN with magnetite nanoparticles,[34] fabricating carbon dots from multi-walled carbon nanotubes,[35] chemo selective hydrogenation using cellulose impregnated with Pd NPs lining the VFD tube,[36] organic synthesis,[37-38] probing the structure of self-organised systems,[39-40] exfoliation and scrolling of *h*-BN and graphite,[41-43] slicing CNTs,[44-45] to mention a few.[41, 46-54] The VFD typically houses a borosilicate glass tube (O.D. diameter 20 mm, I.D. diameter 17.5 mm, 19.5 cm long) open at one end, which is rotated at high speed (up to 9k rpm) and inclined at an angle of 0º to <90º relative to the horizontal position, Fig. 1.[37, 41, 44, 47] The behaviour of MXene in the VFD in the presence of 30% H_2O_2 was explored, which involved varying the flow rate of the solution of MXene in H_2O_2 and the rotational speed of the tube, with the tilt angle fixed at 45 degree as the optimal angle for a plethora of applications of the device.

Results and Discussion

The concentration of MXene in 30% H_2O_2 was varied while fixing the rotational speed at 4k rpm and the flow rate at 0.5 mL/min with the MXene concentration varied, studying 0.1, 0.3, 0.5, 0.7 and 1.0 mg/mL. Of these, 0.5 mg/mL afforded more regular spheroidal particles. We also studied the effect of time on the sonication of MXene in H_2O_2 prior to VFD processing, for 5 mins, 10 mins and 15 mins. The solution turned green after 10 minutes, signifying some oxidation, and this time was then set for all sample preparation for VFD processing.

The flow rate and rotational speed were then systematically varied with the tilt angle for all experiments fixed at 45º, for reasons discussed above, Fig. 1.[32-33, 55] Different flow rates for a concentration of MXene in H_2O_2 at 0.5 mg/mL were used, at 0.25, 0.5, 0.75, 1 and 1.25 mL/min. The optimal flow rate to generate TiO_2NPs/MXene spheres was 0.75 mL/min, with lower yield and less uniform spheres for flow rates of 0.25 and 0.5 mL/min. While spheres also formed at flow rates of 1.0 and 1.25 mL/min they were unstable, disassembling after drop cast on silicon wafer, Fig. S5. For a flow rate of 0.75 mL/min entering the VFD tube, the effect of using different rotational speeds was explored, studying 4, 5, 6, 7, 8 and 9k rpm. Of these, 5k rpm afforded more uniform spheres, in high yield as a suspension exiting the VFD under flow, Fig. S6.

The choice of aqueous H_2O_2 as the solvent for dispersing MXene was to oxidise fragmented MXene to anatase TiO_2 NPs, having previously established that in the absence of hydrogen peroxide, and under an atmosphere of nitrogen, the VFD is effective not only in exfoliating MXene, but also in breaking it down into nanoparticles.[56] These nanoparticles decorate the surface of exfoliated MXene. In the present study, the hydrogen peroxide is indeed effective in converting some of the MXene nanoparticles to anatase TiO_2, which can also decorate the surface of exfoliated MXene along with oxidation of the surface of the MXene, and form spheres of self-assembled TiO_2 NPs and MXene nanoparticles, in generating the two TiO_2 NPs/MXene composites, (i) and (ii) above, Fig. 3 and S1. Different outcomes in the processing arising from varying the rotational speed of the VFD and flow rate in particular, will be determined by differences in fluid dynamic responses which are inherently complex. Indeed, understanding the fluid behaviour in the thin film in the VFD is a major research effort underway, in ultimately being able to predict

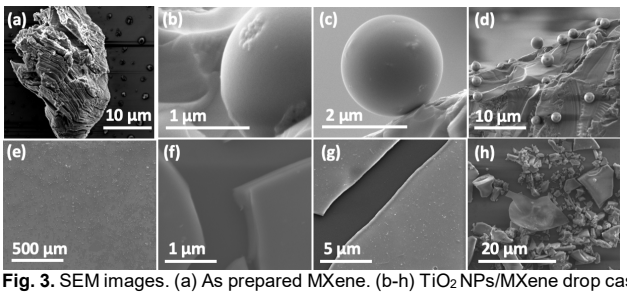

Fig. 3. SEM images. (a) As prepared MXene. (b-h) TiO_2 NPs/MXene drop cast onto silicon wafers, with the material prepared according to the details in Fig. 2. (b-e) Spheres of TiO_2 NPs /MXene(i). (f-h) Sheets of MXene(ii).

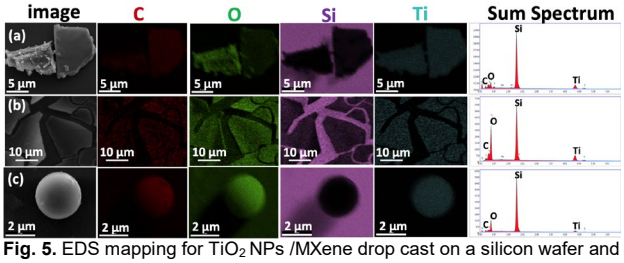

Fig. 5. EDS mapping for TiO_2 NPs /MXene drop cast on a silicon wafer and air dried at 60ºC, optimal VFD parameters, rotational speed 5k rpm, tilt angle 45º and flow rate 0.75 mL/min. (a) MXene as prepared. (b) Sheets of TiO_2NPs/MXene. (c) Spheres of TiO_2NPs /MXene.

10.1002/cnma.201900779

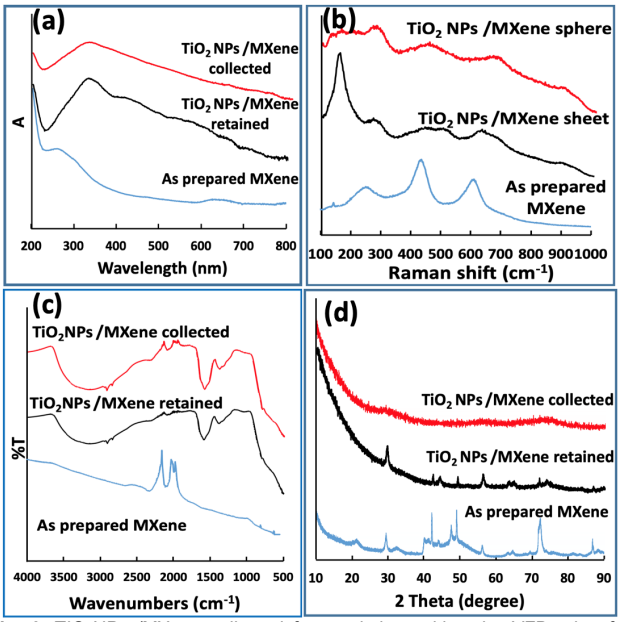

Fig. 6. TiO_2NPs /MXene collected from solution exiting the VFD tube, for MXene at optimal of VFD processing conditions, rotational speed 5k rpm, tilt angle 45º and flow rate 0.75 mL/min followed by drying in air at 60ºC. (a) UV-Vis spectra. (b) Raman spectra for spheres and sheets. (c) ATR-FTIR spectra. (d) Powder X-ray diffraction.

the outcome of any process. In the present study, the mechanoenergy delivered into the thin film has topological effects for generating spheres of the composite material, which is optimal at a flow rate of 0.75 mL/min and 5k rpm rotational speed, but determining how this occurs is challenging.

The dynamic thin film in VFD is also effective in exfoliating other 2D materials including graphene and *h*-BN, with and without scrolling.[41-43] In the present study, treating MXene with aqueous H_2O_2 prior to VFD processing (batch processing) reduced the thickness of the MXene starting material from 10 µm to a few hundred nanometres, presumably driven by surface oxidation along dislocations in the material, Fig. S5(d-f). VFD processing further reduced the thickness of the material, with AFM images showing the presence of 9, 13, 75 and a few hundred nanometre sheets, Fig. 2. The SEM images revealed that the sheets (retained) are topologically smooth, Fig. 3(f-h), S1(f). In this context, we note that the reduction of graphene oxide (rGO) in water via VFD while UV irradiated generates topologically smooth rGO sheets from corrugated GO starting material,[57] and the smoothing here and in the present study presumably comes from the unique high shear fluid flow in the VFD. In addition to the MXene sheets, there are spheres of self-assembled TiO_2/MXene nanoparticles, Fig. 3(b- e), S1(a-e). We note that the shear stress in the VFD is effective for controlling self-assembly, for example in forming cones of fullerene C_{60},[39] and the present result in assembling the spheres adds to this unusual property of fluid flow in the device.

HRTEM of TiO_2NPs/MXene sheets revealed lattice planes of MXene[11] and the size of the TiO_2 nanoparticles (NPs),[58] Fig. 4, S2 and S3. The selected area electron diffraction (SAED) of the material established the presence of anatase TiO_2 NPs on the surface of MXene sheets Fig. 4(d).[29, 59] The EDS spectra and EDS mapping (SEM derived) established the presence of C, O and Ti in the spheres and sheets, Fig. 5, S7 and S8. In addition, the sum spectra are consistent with oxidation of MXene, given the ratio of C to O peaks in the as prepared MXene relative to TiO_2NPs/MXene spheres and sheets, Fig. 5. The Raman spectra of MXene as prepared has three peaks at 259, 435 and 609 cm^{-1},[60] which correspond to titanium carbide in MXene.[61] They are slightly shifted in the Raman spectra of TiO_2NPs/MXene spheres and sheets. The reason for this is a reduction in the number of stacked sheets of MXene in the composite material, from micro to nano thickness, Fig. 2. In addition, the surface functional groups in MXene (−O, −OH and –F) coordinate to titanium in anatase resulting in an increase in vibration energy of Ti-O.[29] A peak in the Raman spectra for anatase at 161 cm^{-1} Fig. 6(b) [31] corresponds to the $E_{g\ (1)}$ vibrational mode.[31, 62] Raman spectroscopy was also used to establish that the spheres and sheets are stable at room temperature, with no change after 60 days, Fig. S11. SEM images and EDX mapping were also consistent with this finding, Fig. S9 and S10. The ATR-FTIR for MXene as prepared has peaks at 632 and 949 cm^{-1} corresponding to Ti-O and C-F stretching frequencies respectively.[63],[64] The VFD processed (collected and retained) material has peaks assignable to MXene, now with additional peaks for H_2O stretching and bending modes at 3380 cm^{-1} and 1608 cm^{-1} respectively.[65] Peaks at 1406 and 813 cm^{-1} are assigned to the lattice vibration of anatase TiO_2 (Ti–O–Ti stretching) and (Ti-O) bending, Fig. 6(c).[65-66]

UV-Vis spectroscopy of the material exiting the VFD tube, and retained in the tube were recorded and compared with as prepared MXene. The VFD processed materials have different spectra, in accordance with their solutions being yellow, with solutions of as prepared MXene being dark grey. This required collecting suspensions of the two materials (retained in the tube and exiting under flow) followed by immediate removal of the solvent *in vacuo*. This was important rather than recording the spectra immediately due to further reaction (oxidation) and evolution of bubbles which reduced the quality of the UV-Vis spectra.[67] The spectra are consistent with the presence of anatase in the composite material, Fig. 6(a).[30, 68-69]

Fig. 6(d) provides the X-ray diffraction data (XRD) for as prepared MXene showing the expected 2θ peaks at 29.4º, 40.6º,

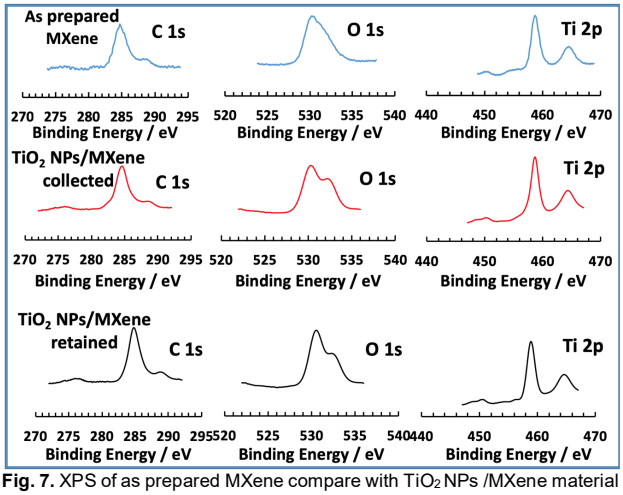

Fig. 7. XPS of as prepared MXene compare with TiO_2 NPs /MXene material collected and retained after drop casting on a silicon wafer and oven dried at 60ºC, for the optimal VFD processing parameters, rotational speed 5k rpm, tilt angle 45º and flow rate of 0.75 mL/min.

42.4º and 72.4º(Co K_α λ= 17889 Å) for the crystal structure of Ti_2CT_x MXene which has hexagonal *P63/mmc* space group and a lattice constant a ≈ 0.3 nm.[70-71] Post VFD processing (after oxidation and fabrication of MXene composites), the XRD of the collected and retained material had peaks corresponding to MXene,[28] with additional peaks for anatase at 2θ 29.6º (101), 44.3º (004), 63.7º (105), 64.9º (211), 74.1 (204) and 83.8º (215).[20], ,[72-73] The peak at 29.6º overlaps with a peak for MXene.[30] The Scherrer equation was used to determine the average size of the anatase TiO_2 NPs retained in the VFD tube, at 18.5 nm.[62]

X-ray photoelectron spectroscopy (XPS) was used as a sensitive characterisation technique for ascertaining any oxidation of MXene. The TiO_2NPs/MXene composite material collected and retained in the VFD had the same XPS spectra for C 1s, O 1s and Ti 2p, Fig. 7. C 1s has peaks at 282.4 eV (C-Ti), 284.8 eV (C-C and C-H) and 288.8 eV (C-O or/and C-F).[69, 72, 74] O 1s has a peak at 530.6 eV (TiO_2), 531.7 eV (C-T-O_x), 532 eV (C-T-$(OH)_x$) and 533.9 (H_2O_{ads}). [69, 74, 75] Ti 2p had peaks corresponding to $Ti^{+2}(2p_{3/2})$, Ti^{+3} $(2p_{3/2})$ for Ti-C (sp^3) at 456 eV and 457.2 eV respectively, and $Ti^{+2}(2p_{1/2})$ and Ti^{+3} $(2p_{1/2})$ for Ti-C (sp^1) at 461 eV and 463.2 eV respectively. [14, 20, 30, 58, 60] The peaks at 459.1 eV and 465.1 eV for Ti-O (sp^3) and Ti-O (sp^1) for TiO_2.[74]

Conclusion

The systematic evaluation of the different operating parameters of the VFD, as a proven strategy for a myriad of applications of the device, proved useful in the present work, with optimal conditions for preparing the spheres and exfoliation at 5k rpm rotational speed, 45º tilt angle and flow rate of a solution of 10 mg of MXene in 20 mL of 30% H_2O_2 at 0.75 mL/min. The oxidation of MXene in 30% aqueous H_2O_2 under shear stress in a VFD is a convenient strategy for decorating layers of MXene with anatase TiO_2 NPs in forming a novel shape composite material with a dramatic reduction in the number of stacked sheets. The processing generates NPs of fragmented MXene which co-assemble with anatase NPs in forming novel spheroidal TiO_2NPs/MXenes composite material, which is stable for extended periods. We note that the ready availability of TiO_2NPs/MXene composites using a VFD offers potential for applications requiring biocompatibility for enzymes,[22] use in modified glassy carbon electrodes for H_2O_2 reduction,[25] nitrite detection,[26] glucose and sodium alanate,[28] Li-ion battery anodes[29] and as photocatalyst.[30]

Experimental Section

Materials. Ti_2AlC powder precursor was obtained commercially (KANTHAL, Maxthal 211 Ti_2AlC). Etching of the aluminium from Ti_2AlC was conducted in a 20% aqueous hydrofluoric acid, HF (Sigma Aldrich), solution for 24 hr at room temperature. The resulting suspension was filtered and washed with deionised water (DI) to reach a pH > 6.[60] The as prepared MXene was dispersed in hydrogen peroxide (30%) from Sigma-Aldrich for all experiments. Control experiments, Fig. S14, used < 100 nm diameter TiO_2 purchased from Aldrich.

Decoration and fabrication of TiO_2NPs/MXene spheres and sheets. The procedure throughout involved dispersing 10 mg of MXene in 20 mL of H_2O_2 (30%) which was then placed in a sonic bath for 10 mins at 6 kHz, whereupon the colour of the solution changed from dark grey to green, Fig. S4(a, b) and Fig. S5(a-f). The solution was then delivered through a syringe to the base of the rotating 20 mm O.D. glass tube using a stainless-steel jet feed. The optimal conditions for preparing this material was a rotational speed of 5k rpm, tilt angle 45º and flow rate 0.75 mL/min for 0.5 mg/mL of MXene in aqueous H_2O_2. Material exiting the glass tube had spheres and sheets of TiO_2NPs/MXene (*ca* 39%), with other material retained in the tube. The natural material was comprised exclusively of sheets of TiO_2NPs/MXene composite material (*ca* 61%). The spheres were about 2 μm ± 0.5 μm in diameter and the average thickness of the sheets was 300 nm ± 200 nm. We make the distinction between the two composite materials as (i) TiO_2 NPs/MXene spheres where spheres of assembled TiO_2 NPs and MXene nanoparticles. The material retained in the tube under flow is (ii) TiO_2 NPs/MXene sheets where exfoliated MXene is decorated with TiO_2 NPs, with the material exiting the tube under flow.

Characterization. TiO_2 NPs/MXene composite materials collected (exiting the tube) and retained in the tube were characterized using scanning electron microscopy (SEM) and EDS (Inspect FEI F50 SEM), atomic force microscopy (AFM - Nanoscope 8.10 tapping mode), Raman spectroscopy (WiTec Alpha 300R $\lambda_{exc.}$=532 nm), XRD (Bruker D8 ADVANCE ECO, Co-Kα, λ=1.7889 Å), ATR-FTIR Perkin Elmer Frontier, HRTEM (FEI Tecnai F20 operated at 200 kV), UV-Vis spectrophotometer Cary 50EST70772 and X-ray photoelectron spectroscopy (XPS) using Mg Kα radiation to determine the elemental composition and the chemical states of all components. The XPS equipment was built by SPECS (Berlin, Germany) with a nonmonochromatic X-ray source. High-resolution scans were recorded for carbon (C), titanium (Ti) and oxygen (O) at a pass energy of 10 eV.

Acknowledgements

The authors gratefully acknowledge financial support from the Iraq Government, Ministry of Higher Education and Scientific Research, and the Australian Research Council and the Government of South Australia. S.K. and N.P.P. (BOE-SAS grant) gratefully acknowledge the financial support provided by LSBU. Use of facilities in the Australian Microscopy & Microanalysis Research Facility (AMMRF) and the Australian National Fabrication Facility (ANFF) at the South Australian nodes of the AMMRF and ANFF under the National Collaborative Research Infrastructure Strategy are also acknowledged.

Keywords: VFD, MXene, anataseTiO_2 nanoparticles, Dynamic thin film, Self-assembly.

Graphic abstract

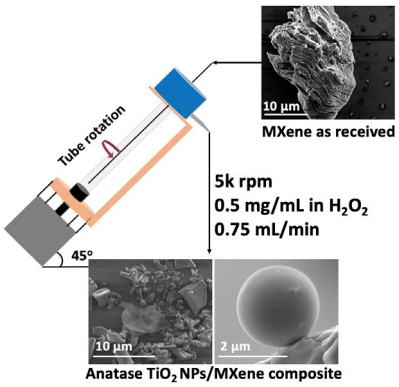

Oxidation of MXene is controlled using 30% hydrogen peroxide in a vortex fluidic device, converting MXene (Ti_2C) into a composite of anatase nanoparticles and MXene, TiO_2 NPs/MXene, with self-assembled fragments of MXene and anatase Ti_2O NPs organised into spheres approximately 2 µm± 0.5 µm in diameter which decorate the surface of exfoliated MXene sheets, from micro to nano dimensions in thickness.

References

[1] M. Naguib, M. Kurtoglu, V. Presser, J. Lu, J. Niu, M. Heon, L. Hultman, Y. Gogotsi, M. W. Barsoum, *Adv.Mater.* **2011**, *23*, 4248-4253.
[2] B. Xu, M. Zhu, W. Zhang, X. Zhen, Z. Pei, Q. Xue, C. Zhi, P. Shi, *Adv.Mater.* **2016**, *28*, 3333-3339.
[3] K. Rasool, M. Helal, A. Ali, C. E. Ren, Y. Gogotsi, K. A. J. A. n. Mahmoud, *ACS Nano* **2016**, *10*, 3674-3684.
[4] G. K. Nasrallah, M. Al-Asmakh, K. Rasool, K. A. J. E. S. N. Mahmoud, *Sci. Nano* **2018**, *5*, 1002-1011.
[5] X. Yu, X. Cai, H. Cui, S.-W. Lee, X.-F. Yu, B. J. N. Liu, *Nanoscale* **2017**, *9*, 17859-17864.
[6] Y. Dall'Agnese, P.-L. Taberna, Y. Gogotsi, P. J. Simon, *J. Phys. Chem. lett.* **2015**, *6*, 2305-2309.
[7] O. Mashtalir, M. Naguib, V. N. Mochalin, Y. Dall'Agnese, M. Heon, M. W. Barsoum, Y. Gogotsi, *Nat. Commun.* **2013**, *4*, 1716.
[8] O. Mashtalir, M. R. Lukatskaya, M.-Q. Zhao, M. W. Barsoum, Y. Gogotsi, *Adv.Mater.* **2015**, *27*, 3501-3506.
[9] M. Khazaei, M. Arai, T. Sasaki, C.-Y. Chung, N. S. Venkataramanan, M. Estili, Y. Sakka, Y. Kawazoe, *Adv. Funct. Mater.* **2013**, *23*, 2185-2192.
[10] M. R. Lukatskaya, O. Mashtalir, C. E. Ren, Y. Dall'Agnese, P. Rozier, P. L. Taberna, M. Naguib, P. Simon, M. W. Barsoum, Y. Gogotsi, *Science* **2013**, *341*, 1502-1505.
[11] X. Wang, S. Kajiyama, H. Iinuma, E. Hosono, S. Oro, I. Moriguchi, M. Okubo, A. Yamada, *Nat. Commun.* **2015**, *6*, 6544.
[12] G. Deysher, S. Sin, Y. Gogotsi, B. Anasori, *Mater. Today* **2018**, *21*, 1064-1065.
[13] Y. Yang, S. Umrao, S. Lai, S. Lee, *J. Phys. Chem. Lett.* **2017**, *8*, 859-865.
[14] F. Du, H. Tang, L. Pan, T. Zhang, H. Lu, J. Xiong, J. Yang, C. Zhang, *Electrochimica Acta* **2017**, *235*, 690-699.
[15] B. Anasori, M. R. Lukatskaya, Y. Gogotsi, *Nat. Rev. Mater.* **2017**, *2*, 16098.
[16] B. Anasori, Y. Xie, M. Beidaghi, J. Lu, B. C. Hosler, L. Hultman, P. R. C. Kent, Y. Gogotsi, M. W. Barsoum, *ACS Nano* **2015**, *9*, 9507-9516.
[17] R. Zou, H. Quan, M. Pan, S. Zhou, D. Chen, X. Luo, *Electrochimica Acta* **2018**, *292*, 31-38.
[18] H. Jiang, Z. Wang, Q. Yang, M. Hanif, Z. Wang, L. Dong, M. Dong, *Electrochimica Acta* **2018**, *290*, 695-703.
[19] X. Jin, S.-J. Shin, N. Kim, B. Kang, H. Piao, J.-H. Choy, H. Kim, S.-J. Hwang, *Nano Energy* **2018**, *53*, 841-848.
[20] X.-T. Gao, Y. Xie, X.-D. Zhu, K.-N. Sun, X.-M. Xie, Y.-T. Liu, J.-Y. Yu, B. Ding, *Small* **2018**, *14*, 1802443.
[21] Y. Gao, L. Wang, Z. Li, A. Zhou, Q. Hu, X. Cao, *Solid State Sci.* **2014**, *35*, 62-65.
[22] J. Zhu, E. Ha, G. Zhao, Y. Zhou, D. Huang, G. Yue, L. Hu, N. Sun, Y. Wang, L. Y. S. Lee, C. Xu, K.-Y. Wong, D. Astruc, P. Zhao, *Coordination Chem. Rev.* **2017**, *352*, 306-327.
[23] L. Lorencova, T. Bertok, J. Filip, M. Jerigova, D. Velic, P. Kasak, K. A. Mahmoud, J. Tkac, *Sensors and Actuators B: Chem.* **2018**, *263*, 360-368.
[24] M. Ghidiu, S. Kota, J. Halim, A. W. Sherwood, N. Nedfors, J. Rosen, V. N. Mochalin, M. W. Barsoum, *Chem. Mater.* **2017**, *29*, 1099-1106.
[25] L. Lorencova, T. Bertok, E. Dosekova, A. Holazova, D. Paprckova, A. Vikartovska, V. Sasinkova, J. Filip, P. Kasak, M. Jerigova, D. Velic, K. A. Mahmoud, J. Tkac, *Electrochimica Acta* **2017**, *235*, 471-479.
[26] H. Liu, C. Duan, C. Yang, W. Shen, F. Wang, Z. J. S. Zhu, A. B. Chemical, *Sensors and Actuators B: Chem.* **2015**, *218*, 60-66.
[27] R. B. Rakhi, P. Nayak, C. Xia, H. N. Alshareef, *Sci. Rep.* **2016**, *6*, 36422.
[28] Y. Fan, Z. Yuan, G. Zou, Q. Zhang, B. Liu, Q. Peng, *Catal. Today* **2018**, *318*, 167-174.
[29] B. Ahmed, D. H. Anjum, M. N. Hedhili, Y. Gogotsi, H. N. Alshareef, *Nanoscale* **2016**, *8*, 7580-7587.
[30] J. Low, L. Zhang, T. Tong, B. Shen, J. Yu, *J. Catal.* **2018**, *361*, 255-266.
[31] M. Naguib, O. Mashtalir, M. R. Lukatskaya, B. Dyatkin, C. Zhang, V. Presser, Y. Gogotsi, M. W. Barsoum, *Chem. Commun.* **2014**, *50*, 7420-7423.
[32] L. Yasmin, X. Chen, K. A. Stubbs, C. L. Raston, *Sci. Rep.* **2013**, *3*, 2282.
[33] J. Britton, K. A. Stubbs, G. A. Weiss, C. L. Raston, *Chem.–A Eur. J.* **2017**, *23*, 13270-13278.

[34] A. H. Mohammed Al-antaki, X. Luo, A. Duan, R. N. Lamb, E. Eroglu, W. Hutchison, Y.-C. Zou, J. Zou, C. L. Raston, *RSC Adv.* **2018**, *8*, 40829-40835.
[35] X. Luo, A. H. M. Al-Antaki, K. Vimalanathan, J. Moffatt, K. Zheng, Y. Zou, J. Zou, X. Duan, R. N. Lamb, S. Wang, Q. Li, W. Zhang, C. L. Raston, *Rea. Chem. Eng.* **2018**, *3*, 164-170.
[36] J. M. Phillips, M. Ahamed, X. Duan, R. N. Lamb, X. Qu, K. Zheng, J. Zou, J. M. Chalker, C. L. Raston, *ACS Appl. Bio Mater.* **2019**, *2*, 488-494.
[37] M. N. Gandy, C. L. Raston, K. A. Stubbs, *Org. Biomol. Chem.* **2014**, *12*, 4594-4597.
[38] S. J. Pye, S. J. Dalgarno, J. M. Chalker, C. L. Raston, *Green Chem.* **2018**, *20*, 118-124.
[39] I. K. Alsulami, T. M. Alharbi, D. P. Harvey, C. T. Gibson, C. L. Raston, *Chem. Commun.* **2018**, *54*, 7896-7899.
[40] K. Vimalanathan, R. G. Shrestha, Z. Zhang, J. Zou, T. Nakayama, C. L. Raston, *Angewandte Chemie* **2017**, *129*, 8518-8521.
[41] X. Chen, J. F. Dobson, C. L. Raston, *Chem. Commun.* **2012**, *48*, 3703-3705.
[42] A. H. M. Al-Antaki, X. Luo, T. M. D. Alharbi, D. P. Harvey, S. Pye, J. Zou, W. Lawrance, C. L. Raston, *RSC Adv.* **2019**, *9*, 22074-22079.
[43] K. Vimalanathan, I. Suarez-Martinez, M. C. R. Peiris, J. Antonio, C. de Tomas, Y. Zou, J. Zou, X. Duan, R. N. Lamb, D. P. Harvey, T. M. D. Alharbi, C. T. Gibson, N. A. Marks, N. Darwish, C. L. Raston, *Nanoscale Adv.* **2019**, *1*, 2495-2501.
[44] T. M. D. Alharbi, K. Vimalanathan, W. D. Lawrance, C. L. Raston, *Carbon* **2018**, *140*, 428-432.
[45] T. M. D. Alharbi, K. Vimalanathan, I. K. Alsulami, C. L. Raston, *Nanoscale* **2019**, *11*, 21394-21403.
[46] X. Luo, P. Smith, C. L. Raston, W. Zhang, *ACS Sustainable Chem. Eng.* **2016**, *4*, 3905-3911.
[47] J. Britton, J. M. Chalker, C. L. Raston, *Chem.–A Eur. J.* **2015**, *21*, 10660-10665.
[48] T. Z. Yuan, C. F. Ormonde, S. T. Kudlacek, S. Kunche, J. N. Smith, W. A. Brown, K. M. Pugliese, T. J. Olsen, M. Iftikhar, C. L. Raston, *ChemBioChem* **2015**, *16*, 393-396.
[49] T. M. D. Alharbi, D. Harvey, I. K. Alsulami, N. Dehbari, X. Duan, R. N. Lamb, W. D. Lawrance, C. L. Raston, *Carbon* **2018**, *137*, 419-424.
[50] A. H. M. Al-Antaki, X. Luo, X. Duan, R. N. Lamb, W. D. Hutchison, W. Lawrance, C. L. Raston, *ACS Omega* **2019**, *4*, 13577-13584.
[51] T. M. D. Alharbi, Y. Shingaya, K. Vimalanathan, T. Nakayama, C. L. Raston, *ACS Appl. Nano Mater.* **2019**, *2*, 5282-5289.
[52] Thaar M. D. Alharbi, A. H. M. Al-Antaki, M. Moussa, W. D. Hutchison, C. L. Raston, *Nanoscale Adv.* **2019**, *1*, 3761-3770.
[53] X. Luo, A. H. M. Al-Antaki, T. M. D. Alharbi, W. D. Hutchison, Y.-c. Zou, J. Zou, A. Sheehan, W. Zhang, C. L. Raston, *ACS Omega* **2018**, *3*, 11172-11178.
[54] X. Luo, A. H. M. Al-Antaki, S. Pye, R. Meech, W. Zhang, C. L. Raston, *ChemPhotoChem* **2018**, *2*, 343-348.
[55] X. Luo, A. H. M. Al-Antaki, D. P. Harvey, Y. Ruan, S. He, W. Zhang, C. L. Raston, *ACS Appl. Mater. Interfaces* **2018**, *10*, 27224-27232.
[56] A.H.M. Al-antaki, S. Kellici, N. P. Power, W.D. Lawrance, C.L. Raston, submitted to Royal Society Open Science with ID: RSOS-192255.
[57] T. M. D. Alharbi, A. R. M. Alghamdi, K. Vimalanathan, C. L. Raston, Chem. Commun. 2019, 55, 11436-11441.
[58] X. Li, X. Yin, M. Han, C. Song, X. Sun, H. Xu, L. Cheng, L. Zhang, *J. Mater. Chem. C* **2017**, *5*, 7621-7628.
[59] J. Wang, S. Dong, H. Li, Z. Chen, S. Jiang, L. Wu, X. Zhang, *J. Electroanalytical Chem.* **2018**, *810*, 27-33.
[60] A. Vaughn, J. Ball, T. Heil, D. J. Morgan, G. I. Lampronti, G. Maršalkaitė, C. L. Raston, N. P. Power, S. Kellici, *Chem-AEur. J.* **2017**, *23*, 8128-8133.
[61] K. J. Cai, Y. Zheng, P. Shen, S. Y. Chen, *CrystEngComm* **2014**, *16*, 5466-5474.
[62] J. Zhang, S. Yan, L. Fu, F. Wang, M. Yuan, G. Luo, Q. Xu, X. Wang, C. Li, *Chinese J. Catal.* **2011**, *32*, 983-991.
[63] Q. Xue, H. Zhang, M. Zhu, Z. Pei, H. Li, Z. Wang, Y. Huang, Y. Huang, Q. Deng, J. Zhou, S. Du, Q. Huang, C. Zhi, *Adv. Mater.* **2017**, *29*, 1604847.
[64] A. Shahzad, K. Rasool, M. Nawaz, W. Miran, J. Jang, M. Moztahida, K. A. Mahmoud, D. S. Lee, *Chem. Eng. J.* **2018**, *349*, 748-755.
[65] Z. Liu, Z. Jian, J. Fang, X. Xu, X. Zhu, S. J. Wu, *Photoenergy* **2012**, *2012*.
[66] E. Alsharaeh, T. Bora, A. Soliman, F. Ahmed, G. Bharath, M. Ghoniem, K. M. Abu-Salah, J. J. C. Dutta, *catalysis* **2017**, *7*, 133.
[67] A. Sarycheva, T. Makaryan, K. Maleski, E. Satheeshkumar, A. Melikyan, H. Minassian, M. Yoshimura, Y. Gogotsi, *J. Phys. Chem. C* **2017**, *121*, 19983-19988.
[68] G. Liu, H. G. Yang, X. Wang, L. Cheng, J. Pan, G. Q. Lu, H.-M. Cheng, *J. Am. Chem. Soc.* **2009**, *131*, 12868-12869.
[69] H. Wang, R. Peng, Z. D. Hood, M. Naguib, S. P. Adhikari, Z. Wu, *ChemSusChem* **2016**, *9*, 1490-1497.
[70] M. Naguib, V. N. Mochalin, M. W. Barsoum, Y. Gogotsi, *Adv. Mater.* **2014**, *26*, 992-1005.
[71] M. Naguib, O. Mashtalir, J. Carle, V. Presser, J. Lu, L. Hultman, Y. Gogotsi, M. W. Barsoum, *ACS Nano* **2012**, *6*, 1322-1331.
[72] A. Ignaszak, C. Song, W. Zhu, J. Zhang, A. Bauer, R. Baker, V. Neburchilov, S. Ye, S. Campbell, *Electrochimica Acta* **2012**, *69*, 397-405.
[73] J. Wang, J. Polleux, J. Lim, B. Dunn, *J. Phys. Chem. C* **2007**, *111*, 14925-14931.
[74] J. Halim, K. M. Cook, M. Naguib, P. Eklund, Y. Gogotsi, J. Rosen, M. W. Barsoum, *Appl. Surf. Sci.* **2016**, *362*, 406-417.
[75] D. Zuo, S. Song, C. An, L. Tang, Z. He, J. Zheng, *Nano Energy* **2019**, *62*, 401-409.